3D Printed Monolithic GRIN Dielectric Loaded Double Ridged Horn Antennas

Karina V. Hoel, Maxim Ignatenko, *Senior Member, IEEE*, Stein Kristoffersen, Erik Lier, *Fellow, IEEE*, and Dejan S. Filipovic, *Fellow, IEEE*

Abstract—Monolithic integration of 3D printed gradient index (GRIN) dielectric loading with a double ridged rectangular horn (SGH) and its impact on antenna performance are demonstrated. Results show that the GRIN loaded horns improve sidelobe levels and beam symmetry, while maintaining good impedance match and relatively high radiation efficiency over more than an octave bandwidth from 7.5 to 18GHz. Moreover, they have low weight and show good robustness to fabrication imperfections. This work paves the way for seamless integration of complex wideband antennas in 3D printed systems such as unmanned aerial vehicles.

Index Terms—3D printed, broadband, copper plating, dielectric loading, GRIN, horns, monolithic, sidelobes, SLS.

I. INTRODUCTION

Additive manufacturing (ADM) enables implementation of geometrically complex structures improving antenna performance and a seamless integration of the antennas with platforms. This paper discusses design and fabrication of a 7.5 to 18GHz 3D printed double ridged pyramidal rectangular horn antenna (SGH) with gradient index (GRIN) dielectric loading, as shown in Fig. 1. The GRIN loading is engineered to decrease sidelobe levels (SLLs) and reduce overall weight of the antenna, thus facilitating its use with unmanned aerial vehicles (UAVs) [1]. The final prototype is monolithic whereby the entire device, including antenna and loading, is manufactured in a single fabrication run.

Horn antennas have been used for over a century in many applications and across microwave and millimeter-wave frequencies [2]; therefore extensive literature is available. When designing horns, one of the most relevant parameters is directivity, which can describe horns with high or low aperture efficiency. In this communication, we focus only on approaches used to reduce the SLLs and/or cross-polarization, that is, horn antennas with inherently low aperture efficiency.

In [3], Lier used dielectric loading in a conical horn to reduce SLLs and cross-polarization below -30dB over 1.6:1 bandwidth, by enabling evanescent wave propagation in the boundary region. Lier and Kildal showed a hard horn in [4], and Kildal formulated the concept of hard and soft surfaces in [5]. Soft horns have the ability to reduce SLLs since the field intensity is tapered over the aperture and approximately zero at the walls [6, 7]. The most common

Karina Vieira Hoel and Stein Kristoffersen are with the Norwegian Defence Research Establishment (FFI), Kjeller 2007 Norway (e-mail: {karina-vieira.hoel, stein.kristoffersen}@ffi.no).

Maxim Ignatenko and Dejan Filipovic are with the Antenna Research Group, Department of Electrical, Computer, and Energy Engineering, University of Colorado Boulder, Boulder, CO 80309 USA (e-mail: {maxim.ignatenko, dejan}@colorado.edu).

Erik Lier is with Lockheed Martin Space, Denver, CO 80125 USA (e-mail: erik.lier@lmco.com).
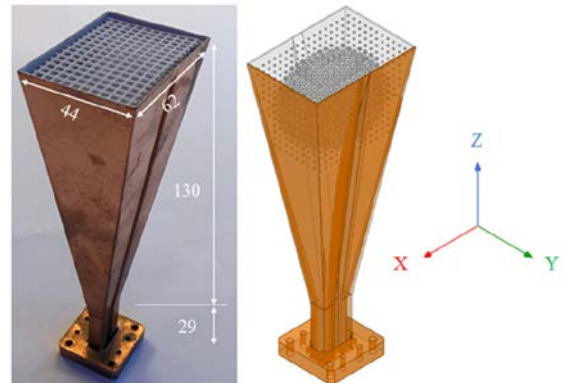
Fig. 1. Monolithic GRIN dielectric loaded horn and HFSS model (all dimensions are in mm).

implementation with corrugations [8] has limited bandwidth due to its resonant structure and requires higher wall thickness, which leads to increased antenna weight. Recently, Lier et al [9, 10] introduced a class of soft horns that utilize low permittivity index (less than 1) metamaterial layer on the walls that eliminates the need for a central dielectric core. This approach shows SLL reduction over 2:1 bandwidth. Many metamaterials and metasurfaces techniques are narrow band, since the design applies around the resonant frequencies [11, 12, 14, 15]; other metamaterials explore the phase compensation and are able to achieve broadband operation [13, 16]. Additional approaches include chokes [17, 18], metals or trifurcation inside the horn [19 - 21], and absorbing materials [22]. A GRIN loaded horn with reduced SLLs over 4 to 6GHz bandwidth is reported in [11]. These techniques are difficult to implement with double ridged horns as the ridges complicate integration. None of these techniques has used 3D printing as the manufacturing process.

In this communication, we utilize GRIN dielectric loading to improve the rotational symmetry of the aperture field over a wide bandwidth (Fig. 2). This way, the SLLs are reduced while high radiation efficiency and good impedance match are maintained over an octave bandwidth. The comparison with other relevant work, focused primarily on reducing SLLs, is shown in Table I.
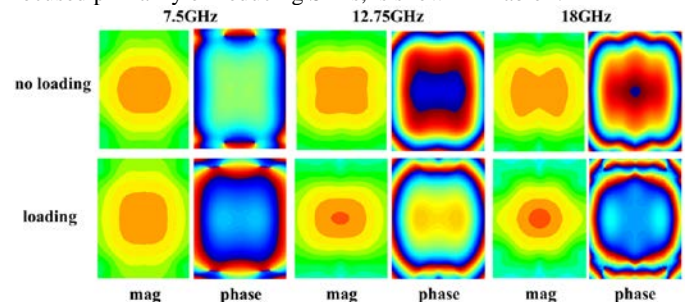

Fig. 2. Aperture electric field distribution (magnitude and phase) for SGH with and without loading. Magnitude plots have scale (0 to 75dB) and phase plots have scale (-90 to 90degrees).

TABLE I
COMPARISON OF SEVERAL LOADED HORNS TO REDUCE SLLs (*SHOWS ONLY SIMULATED RESULTS)

Ref.	Loading Technique	Type of Horn	Additional SLL Reduction	Bandwidth	VSWR	Loading Fabrication	Fabrication Complexity	Costs
[3]	dielectric	conical	~ 10.5dB	1.6:1	< 1.4	machining	moderate	low
[8]	corrugation	conical	~ 10dB	2.25:1	< 2	comp. num. control	high	high
[10]	metamaterial	pyramidal rectangular	~ 10dB	2.1:1	< 1.5	soldering copper wire	moderate	low
[11]	GRIN	pyramidal square	-	1.5:1	< 1.5	PCB	high	moderate
[14]*	metasurfaces	pyramidal rectangular	~ 15dB	1.6:1	< 2	-	high	moderate
[15]*	metasurfaces	pyramidal square	~ 10dB	1.5:1	< 1.5	-	high	high
[16]*	metasurfaces	conical	~ 15dB	1.7:1	-	-	high	moderate
[20]*	metal	pyramidal rectangular	~ 10dB	1.5:1	> 2	-	low	low
Here	GRIN	double ridged pyramidal	~ 15dB	2.4:1	< 1.5	3D printing	low	low

Table I shows that this approach leads to the best combination of bandwidth, SLLs, VSWR at low fabrication complexity. Therefore, in addition to the analysis and design of the GRIN loading, this communication also discusses the details of the fabrication approach. GRIN structures have always been complex to manufacture. The proliferation of low cost 3D printers has enabled easy GRIN fabrication [23 - 25]. This paper demonstrates easy integration of complex, broadband GRIN dielectric loading at low fabrication cost and weight. Even though the study focused on double ridged horns, the concept can be implemented in any type of horn antenna independent of shape or size. A potential drawback is reduced radiation efficiency due to losses induced in the dielectric walls.

II. LOADING ANALYSIS AND DESIGN

A. GRIN Profiles

The study of several volumetric profiles had shown that egg-shell configuration is well suited for GRIN loading of the SGH interior. The loading has maximum permittivity in the center with tapering towards the edge for better matching to the background medium. A number of permittivity profiles were considered; however, due to the similarities in results only three are reported here (Fig. 3). In all cases, the GRIN loading is located close to the horn opening (Fig. 1). To ensure the loading can be fabricated with selective laser sintering (SLS) Nylon PA2200 [26], the relative permittivity changes from 1.7 in the center to 1.15 at the edge in 10 layers. These GRIN profiles help maintaining good impedance match, whereas shaping electric field at the antenna aperture.
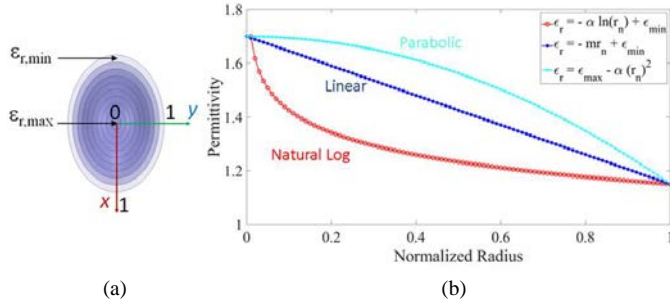

Fig. 3. Discretized shell (a) and permittivity profile approximation (b).

As seen in Fig. 4, all three profiles significantly reduce SLL across most of the band. At frequencies below 9GHz, an increase in SLLs occurs since the loaded horns become more directive. However, the SLLs are located near the 60° angle and therefore, far from the field of view (FOV). The higher reduction in SLLs at higher frequencies is due to the gap (t) between loading and horn wall. According to [3], in order to satisfy the balanced hybrid mode condition for a dielectric core with permittivity ~1.7, t/λ_o needs to be < 0.2. Since t is fixed at

1.5mm, higher values of frequencies will provide the ratio closer to the hybrid mode conditions. However, the loadings here are more complex due to the GRIN patterns, thus some variation is expected. For all following studies, the parabolic profile was chosen.
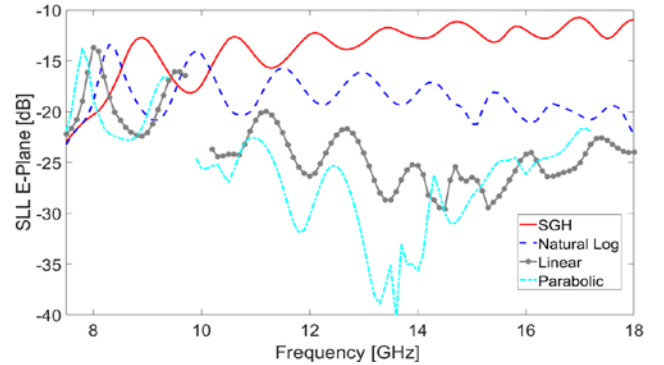

Fig. 4. SLL in E-plane for various GRIN profiles.

B. Unit Cell and Horn Antenna Geometry

The size of the GRIN unit cell is 3.55mm (see inset of Fig. 5), which is 4.7 times smaller than the free space wavelength at the highest frequency of operation [25]. The unit cell is made of three intersecting rods with square profiles and thickness of 0.7mm. At each intersection there is a cube of controllable size.

Simulation of effective permittivity was performed in HFSS using TEM cell and verified with conventional master/slave periodic boundary conditions in the same software. S-parameter data were obtained for different cube-sizes (cs) from 0.7 to 3.55mm and effective permittivity was calculated using the standard retrieval method. The simulated S-parameters also verified that the unit cell of 3.55mm was appropriate for the frequency range studied. The effective relative permittivity (ε_r) can be controlled from 1.15 (grid only) to 2.4 (100% filling) as indicated in Fig. 5.

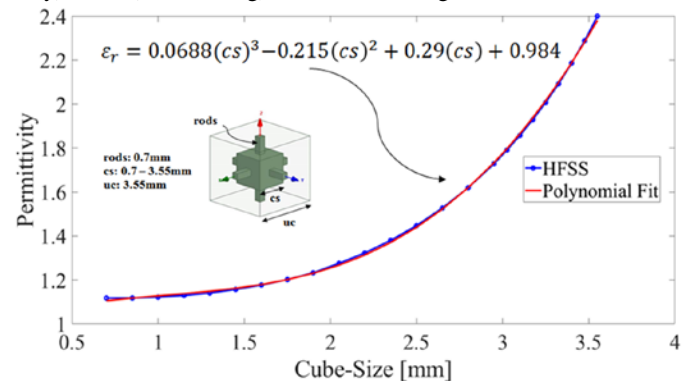$$\varepsilon_r = 0.0688(cs)^3 - 0.215(cs)^2 + 0.29(cs) + 0.984$$

Fig. 5. Extracted permittivity as a function of volume filling factor and corresponding polynomial fit.

A parabolic permittivity profile for GRIN is given as

$$\varepsilon_r = \varepsilon_{r,\max} - (\varepsilon_{r,\max} - \varepsilon_{r,\min})\left(\frac{r}{R}\right)^2 \qquad (1)$$

where $\varepsilon_{r,\max}$ and $\varepsilon_{r,\min}$ are the maximum and minimum effective permittivities, respectively, and R is on an ellipse to accommodate for the geometry of the horn.

$$R = \frac{AB}{\sqrt{B^2 \sin^2 \theta \sin^2 \phi + A^2 \cos^2 \theta \sin^2 \phi + B^2 \cos^2 \phi}} \qquad (2)$$

where A is the minor axis, B is the major axis on the ellipse, θ is the angle x/y plane, ϕ is the angle in z plane.

The dimensions of the horn aperture correspond to 13×17 unit cells. Once the permittivity was calculated the cube-size was evaluated based on the curve shown in Fig. 5. In order to satisfy the balanced hybrid mode condition, a gap between loading and antenna walls was necessary [3]. As mentioned above, a 1.5mm gap was chosen.

The air grooves of the grid reduce the effective loss tangent as shown in Table II. To model the impact of material loss with greater accuracy, the analysis was conducted with the grid.

TABLE II
MEASURED DIELECTRIC CONSTANT FOR PA2200 [25]

Cube-Size	0.7	1.45	2.20	3.55
ε_r	1.15	1.24	1.42	2.4
Tanδ	0.003	0.005	0.007	0.02

C. Loading Analysis and Discussion

For aperture antennas, maximum directivity is achieved with uniform magnitude and phase distributions. For rectangular apertures, this results in SLLs of 13.2dB below beam peak [2]. Any deviation from uniform distribution will change the SLLs. By tapering the amplitude distribution, it is possible to achieve a reduction in SLLs at the expense of lower directivity and a wider main beam. Maintaining the phase uniform allows for the highest possible directivity once tapering in amplitude has taken place.

Horn antennas typically have higher sidelobes in E-plane than in H-plane since the aperture field is more uniformly distributed in E-plane and tapered in H-plane. With the GRIN dielectric loading the objective is to taper the field magnitude in E- and H-planes and to control the phase in order to reduce SLLs in both planes. At the same time directivity drop should be low and radiation efficiency should remain high.
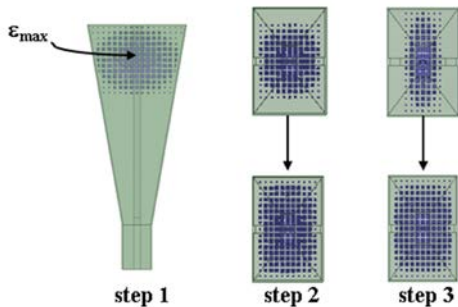

Fig. 6. Description of analysis steps.

In order to develop a systematic analysis of the loading, some parameters were investigated individually. The analysis was performed by first varying only the maximum permittivity in the center while keeping the physical size of the loading fixed (Fig. 6, step 1). Next, a fixed maximum permittivity was chosen and the size of the loading was varied along the x and y dimensions separately (Fig. 6, steps 2 and 3).

1) Step 1 - Permittivity Analysis

Five maximum relative permittivity values ($\varepsilon_{r,\max}$ 1.4, 1.55, 1.7, 2, 2.3 and 2.4) were chosen. For permittivity values < 1.4, the SLLs for the loaded horns approach the values of the SGH. Radiation efficiency at three different frequencies is shown in Fig. 7. As expected, loading reduces gain, particularly at higher frequencies. The dielectric loss accounts for ~1.1dB of gain drop in the worst case, since radiation efficiency goes from 100% for the SGH horn to ~77.4% with permittivity of 2.4 at 18GHz.

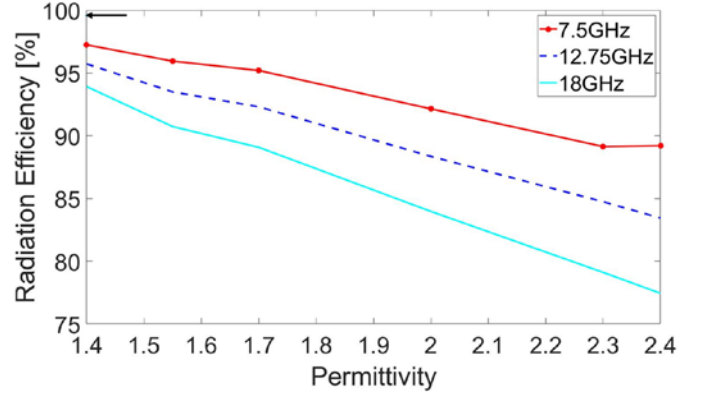

Fig. 7. Radiation efficiency at different frequencies (Arrow indicates SGH).

Fig. 8 shows the HPBW and SLL with respect to the main beam in E-plane. H-plane is less affected, thus not shown here. Clearly, higher permittivity causes wider main beam. Hence, minimum directivity reduction is achieved at lower values of permittivity. SLLs are 15dB better compared to the SGH at higher frequencies and higher permittivity values, since additional magnitude tapering is achieved at the aperture. In fact, the side lobes disappear at higher values of permittivity. As the beam becomes wider, SLLs are completely suppressed. Based on these results, a compromise between radiation efficiency and lower SLLs is needed. Therefore, the maximum permittivity of 1.55 is chosen.
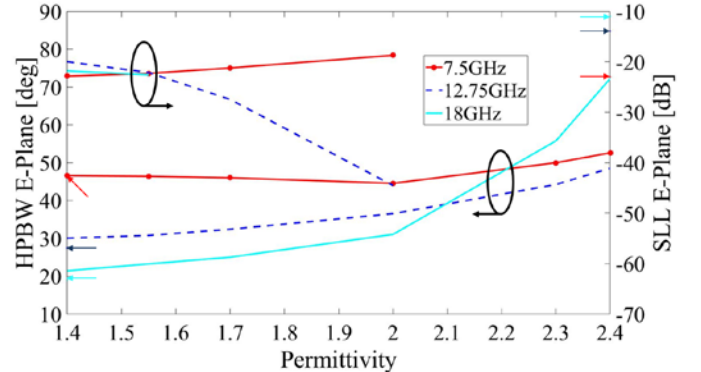

Fig. 8. HPBW and SLLs in E-plane at different frequencies (Arrows indicate SGH).

2) Step 2 – H-plane Scaling

With maximum permittivity of 1.55 in the center fixed, GRIN loading was scaled in the x-dimension with the scaling factor (constant of proportionality C, where $x_{new} = Cx_{old}$) ranging from 0.6 to 1.2, while keeping the y-dimension fixed. The x-axis is in H-plane, thus, higher impact is anticipated there.

Radiation efficiency is higher than 90% for all scaling factors at all frequencies indicating acceptable dielectric losses. Even though noticeable reduction of SLLs in E-plane occurs due to loading, scaling in H-plane does not impact HPBW and SLL. The large opening, scaling factor of 0.6, affects the phase in H-plane, which impacts the radiation pattern especially at higher frequencies.

3) Step 3 – E-plane Scaling

In this study, the *x*-dimension was kept constant and the *y*-dimension was scaled from 0.6 to 1.4. Since the *y*-dimension aligns with *E*-plane, greater impact is expected there. In contrast to scaling in *H*-plane, radiation efficiency reduces for larger scaling factor as shown in Fig. 9. This is less intuitive, but since *y*-variation impacts *E*-field directly, lower values of *y* causes the GRIN loading to be more transparent to electromagnetic waves resembling more the SGH.
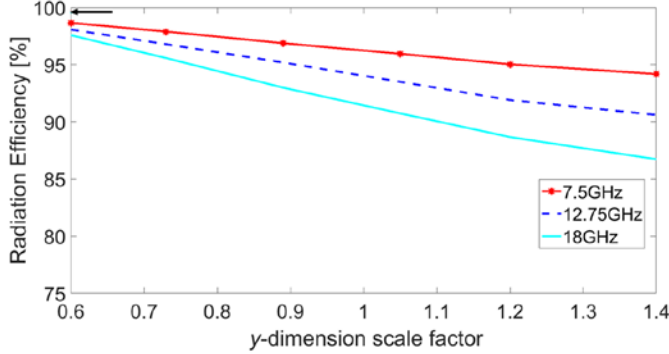

Fig. 9. Radiation efficiency at different frequencies (Arrow indicates SGH).

As seen in Fig. 10, *y*-scaling causes insignificant changes on HPBW in *E*-plane. SLLs at 18GHz monotonically decrease with *y*-scale loading. At mid-band, the SLLs vary within +/- 2dB from the normal value. Once again, a compromise between radiation efficiency and lower SLLs is demonstrated.
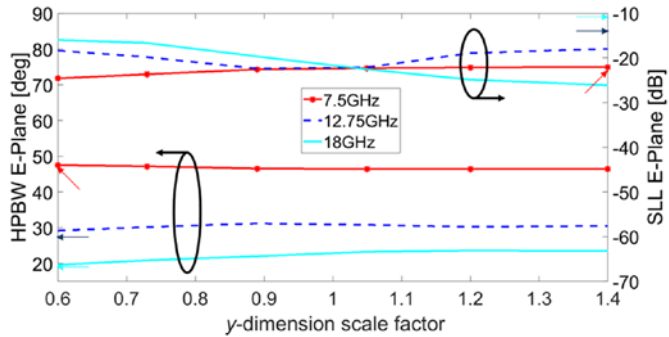

Fig. 10. HPBW and SLLs in *E*-plane at different frequencies (Arrows indicate SGH).

As the *y*-scaling increases, the loading approaches a solid dielectric slab without permittivity variation. The solid slab reduces SLLs [3], nonetheless with less impact at lower frequencies and at the expense of lower radiation efficiency. For larger *y* scale factor, the SLLs go up at 12.75GHz, and they go down at 18GHz.

In summary, there is clear evidence that GRIN loading can significantly improve SLL, particularly at higher frequencies. However, there is little benefit when the profile stretches or shrinks with respect to the horn aperture. Stretching leads to more uniform profile, and the GRIN effect vanishes. Shrinking reduces the dielectric loading, subsequently reducing its effect on horn performance. It is important to note that there are some advantages of using other than 1.55 permittivity values as well. For example, using higher permittivity leads to smaller back and sidelobes at the cost of broader beam and therefore reduced directivity.

Note that positioning the GRIN loading away from the aperture by a couple centimeters had no significant effect on performance. It was also found that the upper half of the loading mainly contributes to SLL reduction, while the lower half mainly affected the impedance match. Stretching the GRIN loading in the *z*-direction did not affect SLLs. It did, however, reduce radiation efficiency due to extra dielectric losses.

III. HORN FABRICATION AND CHARACTERIZATION

A. Horn Fabrication

Two double ridged horn antennas were tested: the monolithic loaded horn, and the hybrid horn, which is the SGH with a separately printed GRIN loading (Fig. 11a). The monolithic loaded horn and the loading were fabricated based on the analysis of the previous section with no scaling in *E*- and *H*-planes and a parabolic profile with permittivity of 1.55 in the center. ADM with SLS technology using Nylon (PA2200) was used to fabricate the parts. The monolithic horn has a 0.7mm wall thickness to hold a 50μm thick copper layer on its exterior. The metal thickness is several skin depths (δ = 0.842μm at 6GHz). The 0.7mm wall thickness is the thinnest recommended for SLS printing.
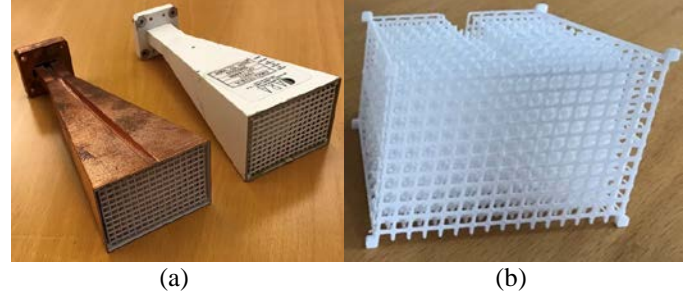

Fig. 11. (a) Monolithic and hybrid horn antennas, and (b) 3D printed GRIN dielectric loading.

The GRIN loading that was printed separately has spacers to maintain 1.5mm gap between horn walls and dielectric loading (Fig. 11b). The spacers are 1.5mm^3 (< λ/10 at 18GHz) and therefore, they have negligible impact on performance.

Completely removing the powder from the grid can be challenging as seen in Fig. 12. This powder and additional fabrication inaccuracies (slightly concave/convex shapes of the cubes) did not affect performance of the horn as seen from simulation and measurement results in the next section.
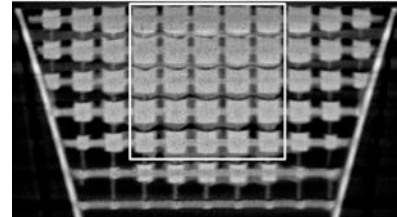

Fig. 12. Computer tomography scan of the 3D printed monolithic horn.

Since the horn was plated on the exterior, the printed wall thickness should be as thin as possible to minimize dielectric losses and avoid undesirable loading. The wall thickness is 0.7mm, which is the thinnest recommended for SLS printing.

The exterior plating also required the antenna flange to be modified. If a regular flange were implemented and plated on the exterior, the flange would constitute a waveguide break, preventing proper operation. To avoid this, several modifications were made. First, a small slit of 1.5mm was added to continue the horn wall inside the flange, such that waveguide section had no break. In order to attach the flange to the antenna, eight small 1.5mm × 1.5mm corners were used. The corners did not affect antenna performance; however, there is still the 0.7mm dielectric wall of the horn inside the WRD750 cross-section as shown in Fig. 13 (left). Second, the slit was terminated by a 0.7mm wall, which was implemented to ensure a good electrical contact between the horn and the coax adapter (Fig. 13, right). Without this wall, the openings due to the ridges affected impedance match. There is a visible impact of this flange on the measurements shown in Fig. 16, though VSWR < 1.5:1.
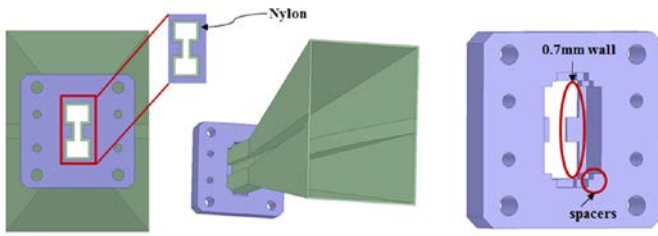
Fig. 13. Flange design for the monolithic horn.

B. Sensitivity Study

The fabrication tolerances were computed with the help of computer tomography (CT). The top view of the 3D printed loaded horn is shown in Fig. 14. Several cube-sizes in different layers were measured in all three dimensions. The worst case variation of +/- 8% was for the smallest cube-size of 0.7mm (varying between 0.644 and 0.756mm). It was found that all other dimensions were maintained well within +/- 5% from the designed model. Ten measurements in each dimension were taken to obtain the values shown in Fig. 14.
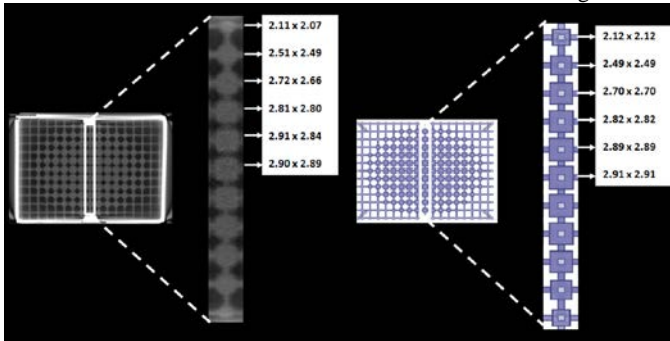

Fig. 14. Computer tomography scan images and measurements (left) and nominal designed block sizes (right). All dimensions are in mm.

To evaluate the sensitivity of the designed GRIN dielectric loading to the fabrication tolerance of +/- 10%, the randomly perturbed GRIN profiles were modeled in HFSS. The cube sizes (*cs*) were calculated based on the curve fit for 24 grid blocks measured in [25]:

$$\varepsilon_r = 0.0688(cs)^3 - 0.2152(cs)^2 + 0.290(cs) + 0.9843 \quad (3)$$

The new random value within the tolerances was calculated as:

$$cs_{new} = cs_1 + (cs_2 - cs_1) \times rand(1) \quad (4)$$

where cs_1 is the lower range (cs_{old} - 10%) and cs_2 is the upper range (cs_{old} + 10%) of the uncertainty and rand(1) generates one uniformly distributed number between 0 and 1 for each cube. The results are compared with the ideal loading performance and it can be concluded that the fabrication tolerance of +/-10% has insignificant effect on the far-field performance as indicated in Fig. 15.
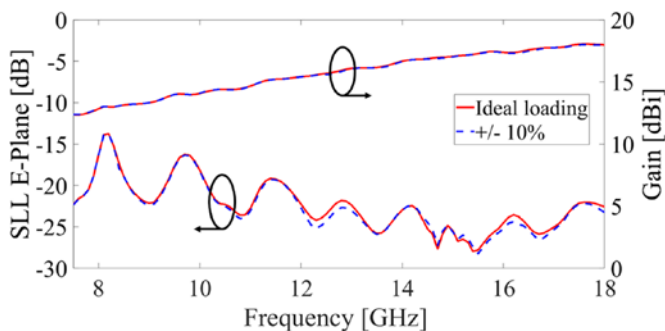

Fig. 15. Impact of tolerances on boresight gain and SLL in *E*-plane.

C. Measurement Results

The impedance match was measured with TRL (thru, reflect, line) calibration performed at the WRD750 waveguide connection. Overall good agreement for VSWR is seen between measured and simulated results in Fig. 16, with an exception for the monolithic horn. The measured results for the monolithic horn can be improved if the flange is 3D printed and plated separately. Having the 0.7mm dielectric wall on the flange impacts the match of the antenna; nevertheless, in all cases VSWR is less than 1.5:1.

The broadside directivity is also shown in Fig. 16. As expected, GRIN loading decreases directivity due to the tapering of the field intensity. Measured and simulated results are in close agreement demonstrating fabrication repeatability and the feasibility of using SLS for monolithic manufacturing. The directivity plot in Fig. 16 shows ~ 2dB loss due to the aperture tapering, this is equivalent to an aperture efficiency of 63% compared to the SGH.
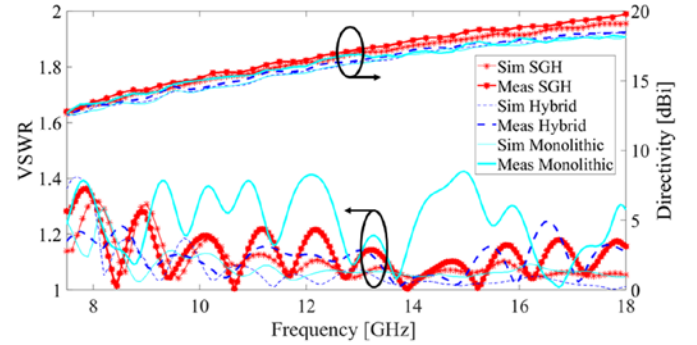

Fig. 16. VSWR and directivity for SGH, hybrid, and monolithic horns.

The radiation efficiency shown in Fig. 17 indicates that some additional dielectric losses occur especially for the monolithic horn due to the extra dielectric wall used for plating on the exterior of the horn. Nevertheless, the radiation efficiency is over 65% (<1dB below SGH) for the entire frequency band. It is clear from Fig. 17 that GRIN dielectric loading greatly reduces SLLs. Measurements verify more than 15dB of SLL improvement at higher frequencies, resulting in radiation patterns with high rotational symmetry. Moreover, the GRIN dielectric loading alone provides minimum gain loss since radiation efficiency > 80% is obtained for $\varepsilon_{r,max}$ = 1.55 at 18GHz, and cross-polarization < -23dB over the entire frequency band.
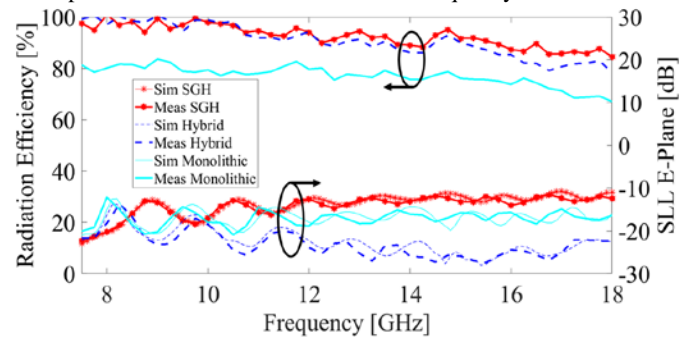

Fig. 17. Radiation efficiency and SLL in *E*-plane for SGH, hybrid, and monolithic horns.

SLLs results also demonstrate that the monolithic horn has higher SLLs compared to the hybrid horn. The reason is the dielectric layer between copper plating and GRIN loading. Simulations indicate that to reduce the SLLs for the monolithic horn, a gap of 3mm between loading and dielectric wall and a permittivity of 1.7 in the center of the loading are necessary [3]. This new loading has negligible impact on VSWR. Radiation efficiency may suffer slightly due to increase in permittivity and dielectric losses. These results are not shown here due to space constraints.

Normalized radiation patterns for SGH, hybrid and monolithic horns in *E*- and *H*-planes are compared in Fig. 18. Good agreement between measured and simulated results is achieved. It is clear that GRIN dielectric loading greatly reduces SLLs. As expected, this effect is mostly pronounced in the *E*-plane.
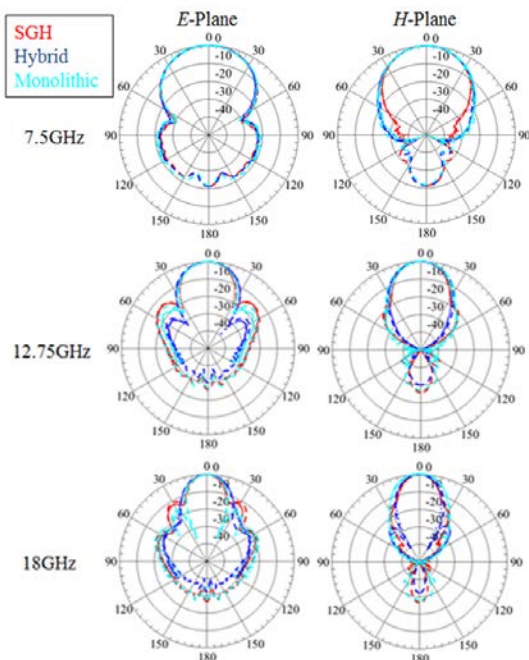

Fig. 18. Radiation pattern for SGH, hybrid, and monolithic horns (dashed lines are simulated whereas dots are measured).

IV. CONCLUSION

The feasibility of the SLS 3D printing approach for fabrication of horns loaded by GRIN dielectric loading is demonstrated. Measurements verify that low SLLs with good impedance match, high radiation efficiency and beam symmetry can be achieved by properly selecting the loading parameters. Design and fabrication details are discussed. For demonstration a double ridged pyramidal horn loaded by GRIN material is fabricated and characterized from 7.5 to 18GHz. Results show that not only can 3D printing provide easy fabrication of complex structures, it can also be utilized to improve the overall performance of complex microwave devices.

REFERENCES

[1] K. V. Hoel, S. Kristoffersen, J. Moen, G. Holm, and T. S. Lande, "Characterization of a 3D printed wideband waveguide and horn antenna structure embedded in a UAV wing," in *2016 10th European Conf. Antennas Propag. (EuCAP)*, Davos, Switzerland, 2016, pp. 1-4.

[2] A. D. Olver, P. J. B. Clarricoats, A. A. Kishk, and L. Shafai, *Microwave Horns and Feeds*, IEEE Press, IEE Electromagnetic Waves Series 39, 1994.

[3] E. Lier, "A dielectric hybrid mode antenna feed: A simple alternative to the corrugated horn, " *IEEE Trans. Antennas Propag.*, vol. 34, no. 1, pp. 21-29, Jan. 1986.

[4] E. Lier, and P. S. Kildal, "A novel type of high-gain horn antenna," in *Proc. 5th Int. Conf. Antennas Propag., ICAP 87*, York, England, Mar. 1987, pp. 431–433.

[5] P. S. Kildal, "Definition of artificially soft and hard surfaces for electromagnetic waves," *Electron. Lett.*, vol. 24, no. 3, pp. 168-170, Feb. 1988.

[6] P. J. Clarricoats, and A. D. Olver, *Corrugated Horns for Microwave Antennas*, Peter Peregrinus, IEE Electromagnetic Waves Series 18, 1984.

[7] E. Lier and T. Schaug-Pettersen, "The strip-loaded hybrid-mode feed horn," *IEEE Trans. Antennas Propag.,* vol. 35, no. 9, pp. 1086-1089, Sep. 1987.

[8] M. Abbas-Azimi, F. Mazlumi and F. Behnia, "Design of Broadband Constant-Beamwidth Conical Corrugated-Horn Antennas - Antenna Designer's Notebook," *IEEE Antennas Propag. Magazine*, vol. 51, no. 5, pp. 109-114, Oct. 2009.

[9] E. Lier and R. K. Shaw, "Design and simulation of metamaterial-based hybrid-mode horn antennas," *Electron. Lett.*, vol. 44, no. 25, pp. 1444-1445, Dec. 2008.

[10] E. Lier, D. H. Werner, C. P. Scarborough, Q. Wu, and J. A. Bossard, "An octave-bandwidth negligible-loss radiofrequency metamaterial," *Nature Materials*, vol. 10, 216–222, 2011.

[11] M. Q. Qi, W. X. Tang, H. F. Ma, B. C. Pan, Z. Tao, Y. Z. Sun & T. J. Cui, "Suppressing side-lobe radiations of horn antenna by loading metamaterial lens," *Nature Scientific Reports 5,* Art. no. 9113, 2015.

[12] X. Chen, Y. Ge and T. S. Bird, "Reduction of sidelobe radiations of the standard pyramidal horn using a thin metamaterial lens," *Electron. Lett.*, vol. 52, no. 24, pp. 1973-1974, 2016.

[13] D. Ramaccia, F. Scattone, F. Bilotti and A. Toscano, "Broadband compact horn antennas by using EPS-ENZ metamaterial lens," *IEEE Trans. Antennas Propag.*, vol. 61, no. 6, pp. 2929-2937, June 2013.

[14] A. Moradi, and F. Mohajeri, "Reduction of SLL in a square horn antenna in presence of metamaterial surfaces by using of particle swarm optimization," in *24th Iranian Conf. on Elec. Eng. (ICEE)*, Shiraz, Iran, 2016, pp. 598-603.

[15] T. Hongnara, K. Schraml, S. Chaimool, P. Akkaraekthalin, and D. Heberling, "Side-lobe reduction of horn antenna using circular patch mushroom-like EBG structure," *German Microwave Conference (GeMiC),* Bochum, Germany, 2016, pp. 413-416.

[16] Q. Wu, C. P. Scarborough, D. Werner, E. Lier, and X. Wang, "Design synthesis of metasurfaces for broadband hybrid mode horn antennas with enhanced radiation pattern and polarization characteristics," *IEEE Trans. Antennas Propag.*, vol. 60, no. 8, pp. 3594-3604, Aug. 2012.

[17] N. Chahat, L. R. Amaro, J. Harrell, C. Wang, P. Estabrook and S. A. Butman, "X-Band Choke Ring Horn Telecom Antenna for Interference Mitigation on NASA's SWOT Mission," *IEEE Trans. Antenna Propag.*, vol. 64, no. 6, pp. 2075-2082, June 2016.

[18] Z. Ying, A. A. Kishk and P. S. Kildal, "Broadband compact horn feed for prime-focus reflectors," *Electron. Lett.*, vol. 31, no. 14, pp. 1114-1115, Jul 1995.

[19] K. K. Chan, C. C. Huang and A. R. Raab, "Dielectric-loaded trifurcated horn for H-plane stacked reflector feed array, " in *Microwaves, Optics and Antennas, IEE Proc. H*, vol. 127, no. 1, 1980, pp. 61-64.

[20] A. Tomaz, J. J. Barroso, and U. C. Hasar, "Side lobe reduction in an X-band horn antenna loaded by a wire medium", *Journal Aerosp. Technol. Manag.*, vol.7, no.3, 2015.

[21] C. Y. Tan and K. T. Selvan, "Performance Comparison of pyramidal horns loaded with metal baffle or with metamaterial," *Progress Electromag. Research C*, vol. 17, 2010.

[22] H. Balegh, B. A. Arand and L. Yousefi, "Side lobe level reduction in horn antennas using graphene," in *24th Iranian Conf. on Elec. Eng. (ICEE)*, Shiraz, Iran, 2016, pp. 1937-1941.

[23] M. Liang, W. R. Ng, K. Chang, K. Gbele, M. E. Gehm and H. Xin, "A 3-D Luneburg lens antenna fabricated by polymer jetting rapid prototyping," *IEEE Trans. Antennas Propag.*, vol. 62, no. 4, pp. 1799-1807, April 2014.

[24] Y. Zhao, Y. Zhang, M. Zheng, X. Dong, X. Duan, and Z. Zhao, "Three-dimensional Luneburg lens at optical frequencies," *Laser and Photonics Reviews*, vol. 10, no. 4, Jun. 2016.

[25] K. V. Hoel and S. Kristoffersen, "Characterization of variable density 3D printed materials for broadband GRIN lenses," in *2017 IEEE Int. Symp. Antennas Propag. & USNC/URSI Nat. Radio Science Meet.*, San Diego, CA, USA, 2017, pp. 2643-2644.

[26] K. V. Hoel, M. Ignatenko, S. Kristoffersen, and D. Filipovic, "Half ellipsoid Luneburg GRIN dielectric lens loaded double ridged horn antenna," in *2018 12th European Conf. Antennas Propag. (EuCAP)*, London, England, 2018, pp. 1-5.